

Recognizing sulfate and phosphate complexes chemisorbed onto nanophase weathering products on Mars using in-situ and remote observations[‡]

ELIZABETH B. RAMPE^{1,*}, RICHARD V. MORRIS², P. DOUGLAS ARCHER JR.³, DAVID G. AGRESTI⁴, AND DOUGLAS W. MING²

¹Aerodyne Industries, Jacobs JETS Contract at NASA Johnson Space Center, 2101 NASA Parkway, Mail Code XI3, Houston, Texas 77058, U.S.A.

²NASA Johnson Space Center, Houston, Texas 77058, U.S.A.

³Jacobs, NASA Johnson Space Center, Houston, Texas 77058, U.S.A.

⁴Department of Physics, University of Alabama at Birmingham, Birmingham, Alabama 35294, U.S.A.

ABSTRACT

Orbital and in-situ data from the surface of Mars indicate that nanophase weathering products are important constituents of martian rocks and soils. Nanophase minerals have the capacity to chemisorb anions like sulfate and phosphate onto their surfaces, but it is not known whether chemisorption is an important or even detectable process via orbital and in-situ observations. The detection of chemisorbed sulfate and phosphate anions on nanophase minerals would constrain the speciation of these anions and past aqueous environmental conditions. Here, we synthesized two nanophase weathering products that are common in terrestrial volcanic soils and have been identified on the martian surface: allophane and nanophase ferric oxide as represented by ferrihydrite. We specifically adsorbed sulfate and phosphate separately onto the nanophase mineral surfaces (4.5 and 1.6 wt% SO_4^{2-} , and 6.7 and 8.9 wt% PO_4^{3-} on allophane and ferrihydrite, respectively) and analyzed the untreated and chemisorbed materials using instruments similar to those on orbital and landed Mars missions (including X-ray diffraction, evolved gas analysis, Mössbauer spectroscopy, and VNIR and thermal-IR spectroscopy). Evolved gas analysis is the optimum method to detect chemisorbed sulfate, with $\text{SO}_{2(g)}$ being released at $>900^\circ\text{C}$ for allophane and $400\text{--}800^\circ\text{C}$ for ferrihydrite. Chemisorbed sulfate and phosphate anions affect the thermal-IR spectra of allophane and ferrihydrite in the S-O and P-O stretching region when present in abundances of only a few weight percent; S-O and P-O stretching bands are apparent as short-wavelength shoulders on Si-O stretching bands. Sulfate and phosphate anions chemisorbed to allophane have small but measurable effects on the position of the OH-H₂O bands at 1.4 and 1.9 μm in near-IR spectra. Chemisorbed sulfate and phosphate anions did not affect the X-ray diffraction patterns, Mössbauer spectra, and visible/near-IR spectra of ferrihydrite. These data suggest that sulfate chemisorbed onto the surfaces of nanophase minerals can be detected with the Sample Analysis at Mars (SAM) instrument on the Mars science laboratory Curiosity rover, and subtle signatures of chemisorbed sulfate and phosphate may be detectable by IR spectrometers on landed missions. The combined use of SAM, the Chemistry and Mineralogy (CheMin) instrument, and the Alpha Particle X-ray Spectrometer (APXS) on Curiosity allows for the most detailed characterization to date of nanophase minerals in martian rocks and soils and the potential presence of chemisorbed anionic complexes.

Keywords: Mars, nanophase minerals, chemisorption, spectroscopy, evolved gas analysis, X-ray diffraction

INTRODUCTION

Precise characterization of chemical weathering products on Mars is important for understanding past and present aqueous environments and for interpreting the habitability of the martian surface. Nanophase weathering products (npWP) are short-range order, nanometer-scale materials and have been detected on the martian surface via in-situ and orbital measurements. In-situ measurements by the instrument payloads onboard the Mars Pathfinder rover and the Mars Exploration Rovers (MER) are

consistent with the presence of nanophase Fe-oxides/oxyhydroxides in the rocks, soils, and dust, including any combination of superparamagnetic hematite and goethite, iddingsite, hisingerite, schwertmannite, akaganeite, ferrihydrite, and a poorly crystalline ferric iron phase associated with unknown amounts of H₂O and OH that is found in terrestrial palagonitic tephra (Morris et al. 2000, 2006a, 2006b). These phases can be present in abundances up to ~66 wt% in rocks and soils at Gusev crater (Ming et al. 2006). Phase models of APXS chemical data from MER in Meridiani and Gusev suggest that allophane, a poorly crystalline aluminosilicate ($\text{Al}_2\text{O}_3 \cdot x\text{SiO}_2 \cdot y\text{H}_2\text{O}$, $x = 0.8\text{--}2$, $y \geq 2.5$), is present in some weathered rocks in abundances of up to ~70 wt% (Clark et al. 2005; Ming et al. 2006). Thermal-infrared spectral models

* E-mail: elizabeth.b.rampe@nasa.gov

[‡] Open access: Article available to all readers online.

of regional Thermal Emission Spectrometer (TES) data suggest that allophane occurs in ~10 vol% abundances over large areas, including Northern Acidalia, Meridiani Planum, Solis Planum, and Aonium-Phrixii (Rampe et al. 2012). X-ray diffraction data measured by the Chemistry and Mineralogy (CheMin) instrument on the Mars Science Laboratory (MSL) Curiosity rover show that amorphous phases are important portions of rocks and soils at Gale crater. Models of CheMin data from the Rocknest sand shadow and the Sheepbed mudstone determined that both samples are composed of ~30 wt% amorphous phases (Bish et al. 2013; Blake et al. 2013; Vaniman et al. 2014), and calculations of the composition of the amorphous component suggest these samples may be composed of 40–50 wt% amorphous phases (e.g., Dehouck et al. 2014; Morris et al. 2015a).

The types of npWP present on the martian surface inform us about the chemical weathering environment. Allophane, a precursor to high-SiO₂ and high-Al₂O₃ clay minerals, is composed of hollow spheres 3–5 nm in diameter. The sphere wall is made up of a rolled octahedral Al-OH sheet with pores, and low-Si allophane has isolated orthosilicate tetrahedra bonded to the octahedral sheet through three Al-O-Si links, with one Si-O-H group pointing inward. The orthosilicate tetrahedra display some polymerization in high-Si allophane (e.g., Parfitt and Hemmi 1980; Parfitt 1990). Allophane and imogolite, a paracrystalline hydrated aluminosilicate, most commonly form from chemical weathering of volcanic glass at pH 5–7 (Wada 1987). Nanophase iron-oxides/oxyhydroxides (npOx) form when ferrous iron (Fe²⁺) is released into solution (usually by dissolution of Fe-bearing silicates like olivine, pyroxene, and volcanic glass) and oxidized to form ferric iron (Fe³⁺). Ferric iron immediately hydrolyzes in the presence of H₂O because of its high affinity for OH⁻ and polymerizes with further hydrolysis, thus forming Fe-oxides/oxyhydroxides (Schwertmann and Taylor 1989). Ferrihydrite (5Fe₂O₃·9H₂O) forms by aqueous alteration in solutions with pH >3 and is composed of spherical particles 3–7 nm in diameter. Under oxidizing conditions, hydration of Fe-bearing glass can result in precipitation of npOx within the glassy matrix. An example is the alteration of basaltic glass to npOx (with an unknown hydration and hydroxylation state) and other alteration products including allophane and halloysite (Morris et al. 1993, 2001).

NpWP are important constituents of weathered basalts and volcanic soils on Earth because they influence physico-chemical properties such as ion adsorption and solute transport. The characteristics of nanophase weathering products that allow them to control these properties are their surface structure and variable surface charge. When these materials are in aqueous fluids, the hydroxylated or hydrated nanophase mineral surface can be negatively or positively charged by desorption or adsorption of H⁺, respectively (Schwertmann and Taylor 1989). The relative amounts of positively and negatively charged sites on the mineral surface are dependent on the pH of the solution, where a decrease in pH favors more positively charged surfaces as more H⁺ is available in solution. Because their surface charges are variable, npWP can adsorb cations and/or anions, which affects the transportation of ions in solution. Ions can be adsorbed by non-specific adsorption (ions retained through electrostatic forces) and specific adsorption or chemisorption (ions retained through formation of covalent bonds) (Nanzoyo et al. 1993). Sulfate and

phosphate anions are specifically adsorbed onto nanophase Fe- and Si/Al-oxides in terrestrial soils, and this chemisorption affects the surface structure of the oxide particles (e.g., Kwon and Kubicki 2004; Ishiguro et al. 2006; Fig. 1).

Although npWP have been identified on Mars through remote and in-situ observations, it is not known if chemisorption has occurred on their surfaces. For example, npOx has been identified at the MER landing sites with Mössbauer spectroscopy, and SO₃ concentrations measured by the alpha particle X-ray spectrometer (APXS) are correlated with npOx abundances (Morris et al. 2006a, 2006b). These data suggest that sulfur could be adsorbed onto the npOx surfaces, but the speciation of sulfur is unknown (e.g., it could instead be present in a separate iron sulfate phase like schwertmannite). Chemical data from APXS in Gusev show that rocks and soils can have up to ~5 wt% P₂O₅ and ~30 wt% SO₃ (Ming et al. 2006), but phase models of the mineralogy of martian rocks and soils assume that none of the phosphate or sulfate is chemisorbed onto weathering products. Calculations of the composition of the X-ray amorphous component of the Rocknest soil at Gale crater show abundances of ~2–3 wt% P₂O₅ and ~10–17 wt% SO₃ (Blake et al. 2013; Dehouck et al. 2014; Morris et al. 2015a), and the X-ray amorphous component in the Sheepbed mudstone has abundances of 2–3 wt% P₂O₅ and 0–11 wt% SO₃ (Vaniman et al. 2014; Dehouck et al. 2014; Morris et al. 2015a). Phosphate and sulfate could be chemisorbed onto the surfaces of nanophase minerals in these samples or present as discrete amorphous phases, such as amorphous sulfate salts (Morris et al. 2015b). The detection and quantification of chemisorbed ions onto weathering products would improve phase models from chemical data and help constrain the secondary mineralogy of the martian surface. Furthermore, the chemisorption of phosphate onto the surface of ferrihydrite can inhibit its transformation to a crystalline Fe-oxide (i.e., hematite or goethite) and generally favors its transformation to hematite over goethite (Gálvez et al.

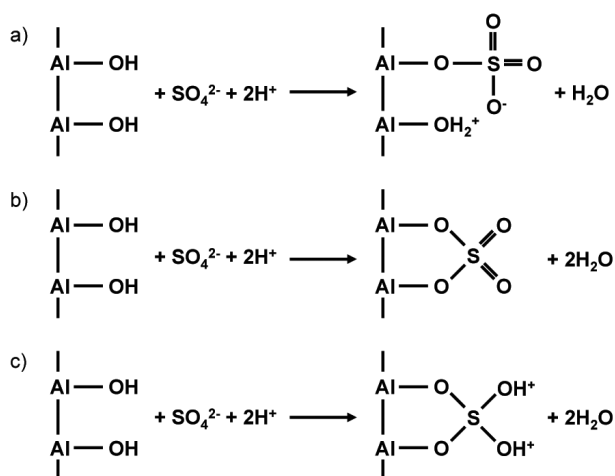


FIGURE 1. Reactions demonstrating specific adsorption of sulfate onto the Al-OH surface of allophane and the formation of different types of sulfate ligands: (a) deprotonated monodentate mononuclear, (b) deprotonated bidentate binuclear, and (c) diprotonated bidentate binuclear. Note that all reactions result in the removal of H₂O. Figure is after Ishiguro et al. (2006) and Kwon and Kubicki (2004).

1999), which may be relevant alteration reactions on Mars (e.g., Catling and Moore 2003; Chevrier et al. 2004).

Here, we report the characterization of chemisorbed phosphate and sulfate anions on synthetic ferrihydrite and allophane using laboratory instruments that have counterparts onboard the MER and MSL rovers; the Phoenix lander; and the Mars Global Surveyor (MGS), Mars Reconnaissance Orbiter (MRO), and Mars Express (MEx) orbiting platforms. Our measurements include visible, near-IR spectroscopy (VNIR), Mössbauer spectroscopy, thermal and evolved gas analysis (EGA), X-ray diffraction (XRD) analysis, and thermal-IR (TIR) emission spectroscopy.

MATERIALS AND METHODS

Nanophase mineral syntheses and ion chemisorption procedures

Two batches of allophane were synthesized from aluminum chloride and sodium orthosilicate solutions using methods adapted from Wada et al. (1979) and Ohashi et al. (2002) to obtain allophane samples with Si/Al molar ratios between 0.5 and 1. Syntheses produced allophane samples having Si/Al molar ratios of 0.7 and 0.9 (determined by atomic absorption spectroscopy). Two-line ferrihydrite was synthesized according to Schwertmann and Cornell (2000). Allophane and ferrihydrite samples were freeze dried, rather than air dried, to achieve very small particle cluster sizes and high surface-to-volume ratios to produce a large surface area for chemisorption.

Sulfate and phosphate chemisorption procedures were adapted from previously published procedures. For allophane, 15 mM solutions of SO_4^{2-} and PO_4^{3-} were prepared using K_2SO_4 and K_2HPO_4 , respectively, and the pH of each solution was adjusted to 5.5 with HCl and KOH (after Jara et al. 2006; Cichota et al. 2007). We selected pH 5.5 for the allophane chemisorption experiments because phosphate is rapidly and strongly chemisorbed to allophane at pH 5–6 (Parfitt 1990). For ferrihydrite, 15 mM solutions of SO_4^{2-} and PO_4^{3-} were prepared using K_2SO_4 and Na_2HPO_4 , respectively, and the pH of the solution was adjusted to 4 with HCl and NaOH (after Willett et al. 1988). We selected pH 4 for the ferrihydrite chemisorption experiments to ensure high surface coverage of phosphate ligands (Willett et al. 1988). The ionic strength of each solution was maintained using KCl as a background electrolyte (0.1 mol/L). The final volume of each solution was 100 mL, and 10 mL of each solution was reserved for ion chromatography to obtain the initial SO_4^{2-} and PO_4^{3-} concentrations. Approximately 1.2 g of either allophane or ferrihydrite was added to the SO_4^{2-} and PO_4^{3-} solutions. An aliquot of each supernatant was reserved for IC after continuously stirring the solutions for 24 h to determine (by difference) the amount of SO_4^{2-} and PO_4^{3-} that had adsorbed on npWP surfaces. The materials were then centrifuged and washed with milliQ water to remove any remaining salts and non-specifically adsorbed ions and oven dried in air at 50 °C. Each chemisorption experiment was performed once. The Si/Al ratio of allophane affects the extent of chemisorption, where there is greater chemisorption with decreasing Si/Al ratio (Parfitt 1990) because silanol groups bond to aluminol groups, thus diminishing the sites to which ligands like sulfate and phosphate can bond (Elsheikh et al. 2009). Phosphate was chemisorbed to allophane with an Si/Al ratio of 0.7, whereas sulfate was chemisorbed to allophane with an Si/Al ratio of 0.9. As such, phosphate likely chemisorbed to a greater extent than would have occurred if phosphate was chemisorbed to allophane with Si/Al = 0.9.

The concentrations of sulfate and phosphate chemisorbed onto allophane and ferrihydrite were quantified by ion chromatography (IC) at NASA Johnson Space Center (JSC) using a Dionex ICS-2000 ion chromatograph. IC analyses of the starting solutions and the solutions after stirring revealed that the allophane had 4.5 wt% chemisorbed SO_4 and 6.7 wt% chemisorbed PO_4 (3.7% SO_3 and 10.0% P_2O_5) and the ferrihydrite had 1.6 wt% chemisorbed SO_4 and 8.9 wt% chemisorbed PO_4 (1.3% SO_3 and 13.3% P_2O_5). These values do not necessarily represent the maximum amount of sulfate and phosphate that can be chemisorbed onto allophane and ferrihydrite; greater amounts of sulfate can be chemisorbed on allophane at pH 4.5 than pH 5.5 (Jara et al. 2006).

Previous studies on phosphate and sulfate chemisorbed ferrihydrite and allophane suggest that these anions formed bidentate surface complexes (Figs. 1b and 1c) on the positively charged allophane and npOx surfaces (e.g., Rajan 1979; Kwon and Kubicki 2004; Khare et al. 2007; Antelo et al. 2010; Zhu et al. 2014). npWP surfaces are positively charged in aqueous solutions with pH less than the

point of zero charge (PZC) of the nanophase mineral. The PZC of allophane and ferrihydrite are ~6.5 and ~8.0, respectively (e.g., Su and Harsh 1993; Antelo et al. 2010). Because we performed our sulfate and phosphate chemisorption experiments at pH 4 and 5.5 for ferrihydrite and allophane, respectively (i.e., below the PZC of both npWP), we infer that the structure of the surface complexes is bidentate. Furthermore, greater concentrations of anionic complexes will chemisorb to positively charged surfaces than to negatively charged surfaces, so performing these experiments below the PZC increases the concentration of surface complexes.

Instrumental methods

Transmission electron microscopy was performed using the JEOL 2500SE 200 kV field-emission scanning-TEM at JSC equipped with a thin window energy-dispersive X-ray (EDX) spectrometer. These measurements were made to ensure samples were amorphous (i.e., no spots indicating crystallinity in electron diffraction patterns) and to assess structural and compositional homogeneity in the samples (e.g., no discrete sulfate or phosphate particles).

XRD analyses were made on a Panalytical X-Pert Pro MPD instrument at JSC. Patterns were measured from 2–80 °2 θ with $\text{CuK}\alpha$ or $\text{CoK}\alpha$ radiation on a traditional spinner stage. The 2 θ range for the MSL XRD instrument (CheMin) is 5 to 50 °2 θ ($\text{CoK}\alpha$ radiation) (Blake et al. 2012).

Thermal and evolved gas analyses were done at JSC using a Netzsch STA 449 F1 Jupiter simultaneous thermogravimetry/differential scanning calorimetry analyzer coupled to a Pfeiffer ThermoStar GSD 320 quadrupole mass spectrometer. Samples were heated from 30 to 1150 °C at 35 °C/min under conditions similar to those on the MSL EGA instrument, Sample Analysis at Mars (SAM): 30 mbar He and 20 sccm flow rate (Mahaffy et al. 2012). The relevant evolved gases (e.g., H_2O , SO_2) were measured by the mass spectrometer and recorded as a function of temperature.

Iron Mössbauer spectroscopy of the untreated and chemisorbed ferrihydrite (our synthetic allophane has no Fe) was performed at JSC at room temperature using a miniaturized Mössbauer spectrometer (MIMOS) II instrument (EPSI, Inc.). The instrument is a backscatter Mössbauer spectrometer with a ^{57}Co source and is the laboratory equivalent of the flight Mössbauer spectrometers on the MER rovers (Klingelhöfer et al. 2003), permitting spectra collected here to be directly compared to MER Mössbauer spectra. Velocity calibrations and least-squares fit of the spectra were done with the computer program MERView and MERFit, respectively (Agresti et al. 2006; Agresti and Gerakines 2009). All spectra were fit with one-, two-, and three-doublet models with peak areas and widths for each doublet constrained to be the same. The Mössbauer parameters derived from the fits are the center shift (CS), quadrupole splitting (QS), full-width at half maximum peak intensity (W), and doublet relative area (A).

VNIR reflectance spectra were measured at JSC with Analytical Spectral Devices FieldSpec3 fiber-optic based spectrometers from 350 to 2500 nm relative to a Spectralon standard and converted to absolute reflectance. Measurements were made in air under ambient temperature and humidity conditions and within a glove box purged with dry- N_2 gas (<110 ppm, H_2O). The H_2O , abundance in the glove box is similar to that experienced on the martian surface (e.g., Martin-Torres et al. 2015).

Spectral measurements within the glove box were made sequentially at 25–35 °C after prolonged (~2–3 weeks) desiccation at 25–35 °C (room temperature), then after heating to 110 and 220 °C on a hot plate. Samples were exposed to higher temperatures when no spectral changes were seen after at least 48 h (i.e., no change in H_2O bands, indicating a stable hydration state). Desiccating conditions removes adsorbed H_2O from the nanophase minerals, permitting examination of their spectral signatures as might be encountered on Mars and detected by orbiting MEx Observatoire pour la Minéralogie, l'Eau, les Glaces et l'Activité (OMEGA) and MRO Compact Reconnaissance Spectrometer for Mars (CRISM) VNIR instruments (Bibring et al. 2004; Murchie et al. 2007). We suggest desiccation at temperatures above ambient is a reasonable surrogate for desiccation at lower temperatures over geologic timescales on Mars.

Thermal-IR emission spectra of compressed pellets (as opposed to loose powders) of untreated and chemisorbed npWP were collected at the Mars Space Flight Facility at Arizona State University using a Nicolet Nexus 670 spectrometer configured to measure emitted energy (Christensen and Harrison 1993; Ruff et al. 1997). Pellets were created by compressing ~0.1 g of particulate material to ~70 MPa (uncorrected for friction) in a hydraulic press for 3 min (Michalski et al. 2005). Pellets were 1 cm in diameter and a few millimeters thick, placed in copper sample cups painted black so that they behave as a spectral blackbody, and heated to 80 °C before and during the experiments to increase the signal-to-noise ratio. Spectra were scanned 270 times over the course of ~4 min, from 200–2000 cm^{-1} with 2 cm^{-1} spectral resolution. Blackbodies at 70 and 100 °C were measured

to calibrate raw data to radiance (Christensen and Harrison 1993). Heating likely caused partial dehydration of the samples; however, spectral bands from H₂O do not interfere with bands in ferrihydrite, allophane, sulfate, or phosphate over the scanned range. Radiance spectra were transformed to emissivity spectra by normalizing to the Planck curve corresponding to the sample temperature (Ruff et al. 1997).

RESULTS

Transmission electron microscopy

Transmission electron photomicrographs show that the sulfate- and phosphate-chemisorbed npWP samples lack long-range crystallographic order and are homogenous (Fig. 2). Allophane samples are comprised of clusters of nanometer-scale particles up to a few micrometers in diameter, and high-resolution images show a lack of lattice fringes (Figs. 2a and 2c). Selected-area electron diffraction (SAED) patterns show two diffuse rings (Fig. 2b), corresponding to *d* spacings of ~ 2.2 and ~ 3.4 Å. TEM of chemisorbed allophane samples show that they are morphologically and structurally similar to previous studies of natural and synthetic allophane (e.g., Wada 1989; Ohashi et al. 2002; Rampe et al. 2012). Ferrihydrite samples are similarly comprised of clusters of nanometer-scale spherules (Fig. 2d), and high-resolution TEM show some small areas with lattice fringes (Fig. 2f), showing areas of incipient crystallinity. SAED patterns show two bright rings (Figs. 2e), corresponding to *d*-spacings of ~ 1.5 and 2.6 Å. TEM of chemisorbed ferrihydrite samples are morphologically and structurally similar to previous studies of natural and synthetic ferrihydrite (e.g., Schwertmann and Taylor 1989; Janney et al. 2000). TEM confirms that neither the

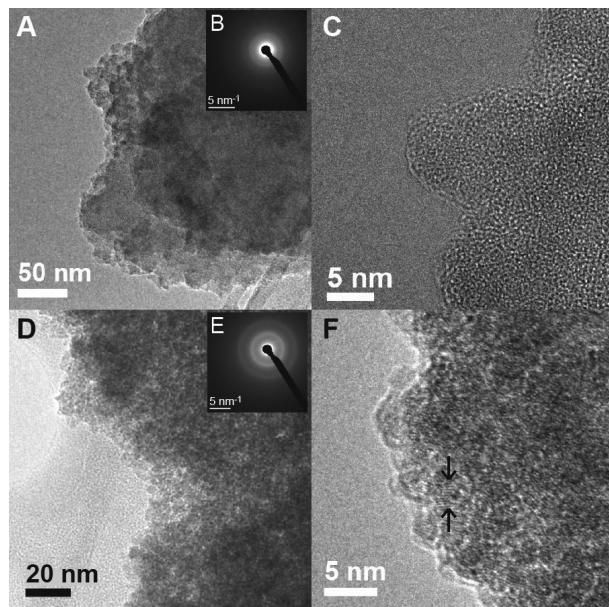


FIGURE 2. (a–c) Transmission electron microscopy (TEM) of phosphate-chemisorbed allophane: (a) TEM image of allophane cluster, (b) selected-area electron diffraction (SAED) of allophane, and (c) high-resolution TEM image of allophane. (d–f) Transmission electron microscopy of phosphate-chemisorbed ferrihydrite: (d) TEM image of ferrihydrite cluster, (e) SAED of ferrihydrite, and (f) high-resolution TEM image of ferrihydrite with small areas of lattice fringes denoted by black arrows. Results of TEM of sulfate-chemisorbed npWP samples are similar.

chemisorbed allophane nor the chemisorbed ferrihydrite contain discrete sulfate or phosphate phases.

X-ray diffraction

The broad XRD peaks with low intensities for untreated synthetic allophane and ferrihydrite demonstrate that these materials lack long-range crystallographic order. The peaks for allophane occur at 1.4, 2.2, and 3.4 Å (Fig. 3a), consistent with previous XRD studies of natural and synthetic allophane (Wada 1989) and the rings measured in TEM-SAED patterns (Fig. 2b). The XRD peak at 1.4 Å was not observed in TEM-SAED because it is very weak. The allophane pattern also displays a low-angle peak at ~ 24 Å, which has been attributed to diffraction off of closely packed spheres of allophane (van der Gaast et al. 1985). Previous studies of natural and synthetic allophane and imogolite have noted that this peak becomes more intense with dehydration (van der Gaast et al. 1985; Bishop et al. 2013) because as adsorbed water is removed, the spherules become more tightly packed. This phenomenon occurs in chemisorbed allophane because the chemisorption of ions to the allophane surface results in the removal of H₂O adsorbed to the surface (Fig. 1). The peaks for

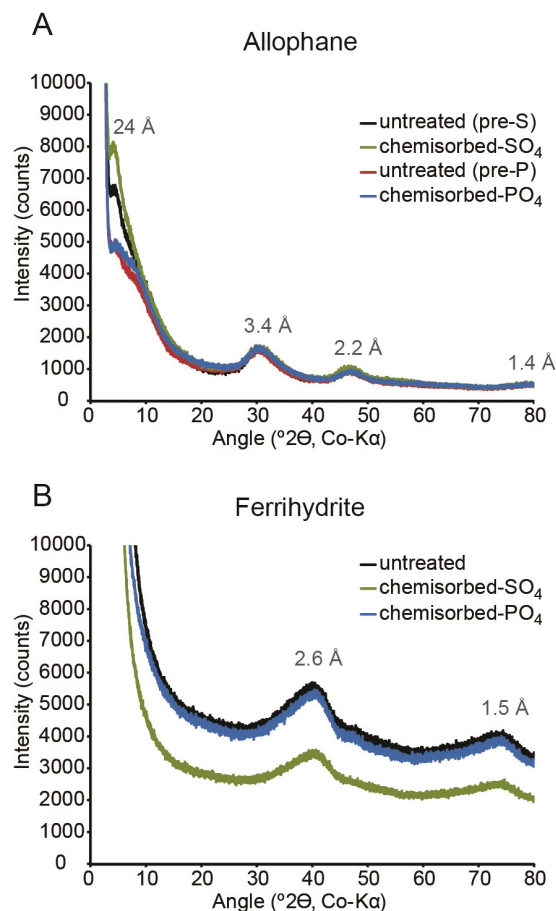


FIGURE 3. X-ray diffraction patterns of (a) untreated, phosphate-chemisorbed, and sulfate-chemisorbed allophane, and (b) untreated, phosphate-chemisorbed, and sulfate-chemisorbed ferrihydrite. Allophane samples were measured under CuK α radiation, and the patterns were calculated for CoK α .

2-line ferrihydrite occur at 1.5 and 2.6 Å (Fig. 3b), consistent with previous XRD studies of natural and synthetic 2-line ferrihydrite (e.g., Schwertmann and Cornell 2000; Bishop and Murad 2002) and the rings measured in TEM-SAED patterns (Fig. 2e). Patterns from both npWP show a rise in intensity at low angles. The chemisorption of sulfate and phosphate onto allophane and ferrihydrite does not affect the position of the XRD peaks and generally does not affect the peak intensities (Fig. 3). The only difference induced by the chemisorption of sulfate or phosphate is the intensity of the low-angle allophane peak at ~ 24 Å; this peak becomes more pronounced with the chemisorption of sulfate or phosphate and desorption of H_2O .

Thermal and evolved gas analysis

Evolved gas analyses of the untreated samples show intense releases of gas with mass/charge (m/z) equal to 18 (i.e., H_2O). EGA traces of m/z 18 from untreated allophane show two, broad low-temperature releases followed by a steady decrease in the amount of H_2O released with increasing temperature. The low-temperature release occurs from ~ 50 – 400 °C, with peak releases

at ~ 120 and 275 °C (Fig. 4a). These peaks relate to the removal of adsorbed and structural H_2O , respectively (Borchardt 1989; Wada 1989). EGA traces of m/z 18 from untreated ferrihydrite show one broad temperature release from ~ 50 – 350 °C with a maximum at ~ 120 °C (Fig. 4b). This broad release in the EGA data are from the loss of adsorbed and structural H_2O and structural OH in ferrihydrite as it transforms to hematite (Schwertmann and Cornell 2000).

EGA data of m/z 18 from sulfate- and phosphate-chemisorbed allophane are similar to the untreated allophane. The m/z 18 EGA data from sulfate- and phosphate-chemisorbed ferrihydrite, however, differ from the untreated ferrihydrite data because a sharp release is present at a peak temperature of 440 °C (Fig. 4b). The temperature of this release corresponds to the temperature at which ferrihydrite completely transforms to hematite, and this transition is visible in the corresponding differential scanning calorimetry data (data not shown). The presence of chemisorbed sulfate or phosphate on the surface of ferrihydrite thus inhibits the transition to hematite until about 440 °C by preventing the aggregation and intimate contact of ferrihydrite grains (Gálvez et al. 1999) so that the transition from ferrihydrite to hematite is not gradual as it is in the untreated ferrihydrite sample, but instead is rapid with H_2O evolution over a narrow temperature interval.

Evolved gas analyses of m/z 64 (i.e., SO_2) from sulfate-chemisorbed allophane show a release with an onset temperature at ~ 900 °C and a peak release at ~ 960 °C (Fig. 4). The sulfate-chemisorbed ferrihydrite EGA data show releases of SO_2 at ~ 400 , 490 , and 700 °C. Evolved gas analyses of phosphate-chemisorbed allophane and ferrihydrite do not show definitive evidence of the presence of phosphate because phosphate is not released as a gas below the maximum temperature of our experiments (1150 °C) (e.g., Frost et al. 2004; Gallini et al. 2005). Untreated ferrihydrite data display a m/z 30 release (NO) at ~ 200 °C from adsorbed nitrate (data not shown), which we interpret as a vestige of the synthesis from $\text{Fe}(\text{NO}_3)_3$ (Šubrt et al. 1992).

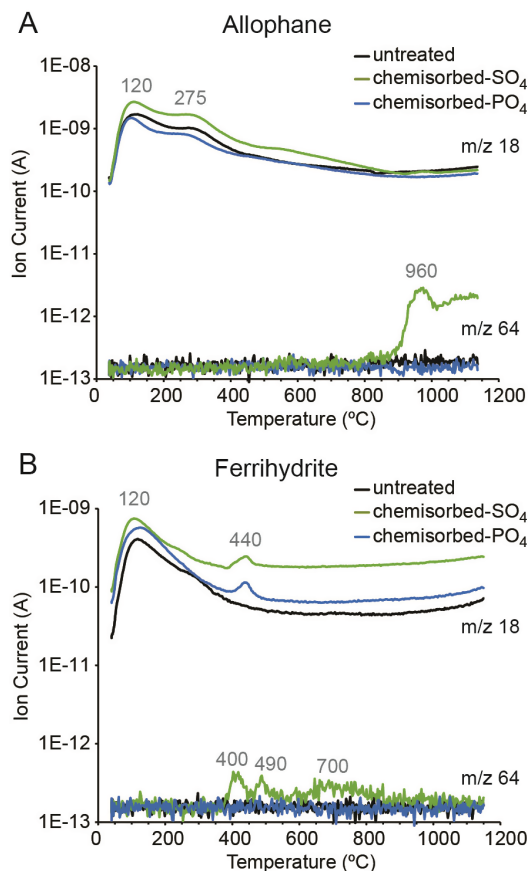


FIGURE 4. Evolved gas analysis data of (a) m/z 18 [$\text{H}_2\text{O}_{(\text{g})}$] and m/z 64 [$\text{SO}_{2(\text{g})}$] measured from untreated, sulfate-chemisorbed, and phosphate-chemisorbed allophane, and (b) m/z 18 [$\text{H}_2\text{O}_{(\text{g})}$] and m/z 64 [$\text{SO}_{2(\text{g})}$] measured from untreated, sulfate-chemisorbed, and phosphate-chemisorbed ferrihydrite. Samples were measured under Sample Analysis at Mars-like operating conditions.

Mössbauer spectroscopy

There were no detectable differences among the Mössbauer spectra for the untreated and chemisorbed ferrihydrite samples. As a representative example of the spectra from all samples, we show in Figure 5 the spectrum for sulfate-chemisorbed ferrihydrite with a three-doublet fit. The values of the Mössbauer parameters are compiled in Table 1 for one- and three-doublet fits. The quality of the fit improves with additional doublets (decreasing values of χ^2), but the values of CS and QS for each doublet do not change within error for untreated and chemisorbed samples.

Visible/near-infrared spectroscopy

The VNIR reflectance spectrum of untreated allophane measured in lab air shows broad spectral bands with minima near 0.95 , 1.4 , 1.9 , and 2.2 μm (Fig. 6a). The first three minima result from overtones and combinations of the fundamental stretching and bending vibrations of the H_2O molecule and, for the 1.4 μm minimum only, overtones from the OH stretching vibration of the (Si,Al)OH functional group. The minimum near 2.2 μm is a combination of the bending and stretching vibration of the OH in the (Si,Al)OH functional group. Only the minimum near 1.9 μm requires the presence of the H_2O molecule (i.e., H-O-H

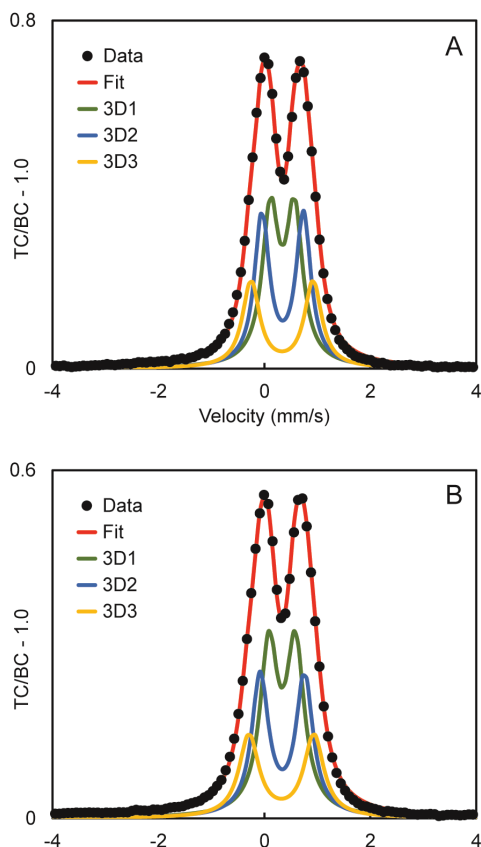


FIGURE 5. Three-doublet fit for Mössbauer spectra of sulfate-chemisorbed 2-line ferrihydrite equilibrated (a) in lab air and (b) at 220 °C under desiccating conditions [dry $N_{2(g)}$]. TC = total counts; BC = baseline counts.

TABLE 1. Mössbauer parameters (room temperature) calculated from least-squares fitting procedure for one- and three-doublet models for 2-line ferrihydrite without adsorbed anions and with adsorbed sulfate and phosphate anions

Adsorbed anion	Ambient			Desiccated 220 °C		
	None	Sulfate	Phosphate	None	Sulfate	Phosphate
One-doublet model						
CS (mm/s)	0.35(2)	0.34(2)	0.34(2)	0.34(2)	0.34(2)	0.34(2)
QS (mm/s)	0.73(2)	0.72(2)	0.74(2)	0.75(2)	0.75(2)	0.81(2)
FWHM (mm/s)	0.51(2)	0.52(2)	0.55(2)	0.54(2)	0.56(2)	0.57(2)
A (%)	100	100	100	100	100	100
Three-doublet model						
<i>Ferric doublet 1</i>						
CS (mm/s)	0.34(2)	0.34(2)	0.34(2)	0.34(2)	0.34(2)	0.34(2)
QS (mm/s)	0.45(2)	0.45(2)	0.43(2)	0.53(2)	0.50(2)	0.56(2)
FWHM (mm/s)	0.36(2)	0.38(2)	0.37(2)	0.40(2)	0.41(2)	0.41(2)
A (%)	36(4)	40(5)	33(6)	53(4)	42(5)	51(2)
<i>Ferric doublet 2</i>						
CS (mm/s)	0.34(2)	0.34(2)	0.34(2)	0.33(2)	0.34(2)	0.34(2)
QS (mm/s)	0.78(2)	0.78(2)	0.77(2)	0.91(2)	0.84(2)	0.96(2)
FWHM (mm/s)	0.33(2)	0.34(3)	0.36(3)	0.35(2)	0.39(2)	0.35(2)
A (%)	38(6)	36(8)	38(9)	31(6)	34(8)	31(3)
<i>Ferric doublet 3</i>						
CS (mm/s)	0.34(2)	0.33(2)	0.33(2)	0.32(2)	0.32(2)	0.32(2)
QS (mm/s)	1.17(2)	1.17(2)	1.18(2)	1.31(2)	1.22(2)	1.39(2)
FWHM (mm/s)	0.38(2)	0.39(2)	0.44(2)	0.38(2)	0.45(2)	0.39(2)
A (%)	24(3)	24(4)	29(4)	16(2)	24(4)	18(2)

Notes: CS = center shift relative to metallic iron foil at room temperature; QS = quadrupole splitting; FWHM = full-width at half maximum intensity; A = sub-spectral area. Uncertainty of the final digit given in parentheses.

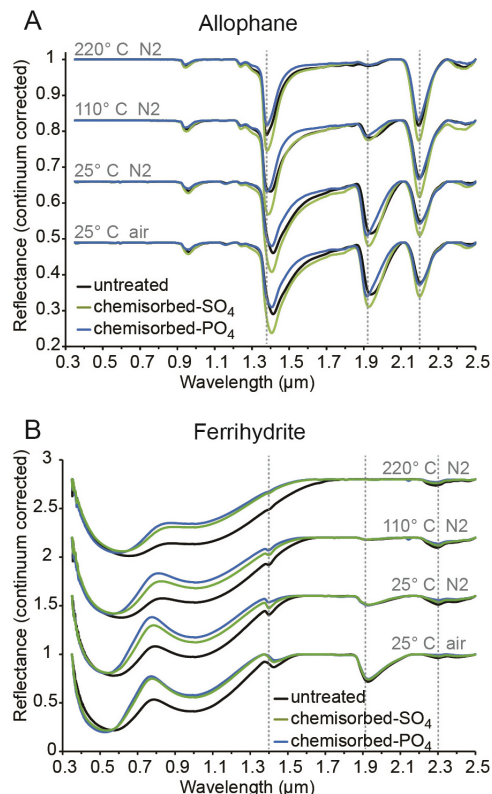


FIGURE 6. (a) Visible/near-infrared reflectance spectra of untreated, sulfate-chemisorbed, and phosphate-chemisorbed allophane measured under ambient conditions and in a $N_{2(g)}$ -purged glove box at 25, 110, and 220 °C. Dashed vertical lines are at 1.38, 1.91, and 2.20 μm . Spectra are offset for clarity. (b) Visible/near-IR reflectance spectra of untreated, sulfate-chemisorbed, and phosphate-chemisorbed ferrihydrite measured under the same conditions as the allophane spectra. Dashed vertical lines are at 1.40, 1.91, and 2.30 μm . Spectra have been continuum removed and are offset for clarity.

stretching and bending vibrations). The band positions reported here are consistent with those previously reported for natural and synthetic allophane (e.g., Bishop et al. 2013). The band near 1.4 μm is a doublet with minima near 1.38 and 1.40 μm (from the OH and H_2O overtone, respectively), as was reported by Bishop et al. (2013), with greater contributions from the band at 1.38 μm as the samples became more desiccated.

The VNIR reflectance spectrum of untreated ferrihydrite measured in lab air shows broad spectral features with minima near 0.6, 1.0, 1.4, 1.9, and 2.3 μm (Fig. 6b). The minimum near 1.9 μm results from overtones and combinations of the fundamental vibrations of the H_2O molecule, as for allophane. The bands near 1.4 and 2.3 μm result from the Fe^{3+} -OH bending-stretching combination vibrations, and the band near 1.4 μm also has a contribution from the H_2O stretching overtone. Broad minima near 0.6 and 1.0 μm are from Fe^{3+} electronic transitions. The band positions reported here are consistent with those previously reported for natural and synthetic ferrihydrite (e.g., Bishop and Murad 2002).

With desiccation by exposure to dry $N_{2(g)}$ and with and without mild heating (Fig. 6), the amount of H_2O diminishes and is nearly

absent from spectra for the allophane and ferrihydrite samples heated to 220 °C on the basis of the intensity of the 1.9 μm spectral feature. For the 1.4 μm spectral feature, the corresponding changes with desiccation are decreasing intensity and a shift of the band minimum to shorter wavelengths (1.43 to 1.38 μm and 1.43 to 1.40 μm for allophane and ferrihydrite, respectively). These intensity and position changes result from decreasing contributions of the fundamental H_2O stretching overtone to the spectral feature as the H_2O abundance decreases (on the basis of decreasing 1.9 μm band intensity) relative to the contributions from (Si,Al)-OH and Fe-OH. Band minima of the 1.4 and 1.9 μm features are similar for the untreated, sulfate-chemisorbed, and phosphate-chemisorbed ferrihydrite at each stage of desiccation. However, these band minima are measurably different between the untreated, sulfate-chemisorbed, and phosphate-chemisorbed allophane at each stage of desiccation, such that the position of the bands of the untreated allophane are at the longest wavelength and those of the phosphate-chemisorbed allophane are at the shortest wavelength (Table 2).

For the 2.1 to 2.5 μm spectral region, the spectra of sulfate- and phosphate-chemisorbed allophane samples exposed to the same temperature and humidity conditions are similar to their untreated counterparts. It is unlikely that bands from vibrations of S-O and P-O bonds would be detected with VNIR spectroscopy because these features would result from at least the fourth overtone of such vibrations (Hunt et al. 1971).

The spectral features in the 2.1 to 2.5 μm region for the untreated and chemisorbed ferrihydrite samples are much weaker in comparison to allophane (Fig. 6). The strongest feature is located at 2.30 μm (from Fe^{3+} -OH), and its intensity is not markedly dependent on the extent of desiccation, although it broadens giving the appearance of an unresolved envelope of more than one band. The phosphate-chemisorbed ferrihydrite spectra measured under desiccating conditions have a weak band centered at 2.15 μm . We do not have sufficient information to assign this band, but it occurs in the same spectral region as bands attributed to combinations of OH stretching and bending vibrations (Bishop and Murad 2002).

The broad minima near 1.0 μm in the spectra of chemisorbed ferrihydrite have lower reflectance than the minimum in the spectrum of untreated ferrihydrite. We hypothesize that the chemisorption of spectrally neutral ligands (SO_4 and PO_4)

caused a slight increase in albedo, leading to the diminished reflectance near 1.0 μm .

Thermal emission spectroscopy

TIR spectra of compressed pellets of untreated allophane have broad bands at 950 cm^{-1} from Si-O stretching vibrations, 550 cm^{-1} from Al-O-Si deformation vibrations, 420 cm^{-1} from Si-O bending vibrations, and 340 cm^{-1} from Al-OH deformation vibrations (Fig. 7a) (Rampe et al. 2012). The Si/Al ratio can affect the position of the Si-O stretching vibration, where the band is shifted to higher wavenumbers with increasing Si/Al ratio (e.g., Rampe et al. 2012); however, there were no differences between the TIR spectra of the two allophane samples we synthesized here. Sulfate- and phosphate-chemisorbed allophane have corresponding spectral features, but with a weak shoulder on the high-frequency side of the Si-O stretching vibration at ~ 1050 – 1200 cm^{-1} and a shoulder on the high-frequency side of the Al-O-Si deformation vibration at 600 cm^{-1} . The shoulder at 1050–1200 cm^{-1} is from S-O and P-O stretching and bending

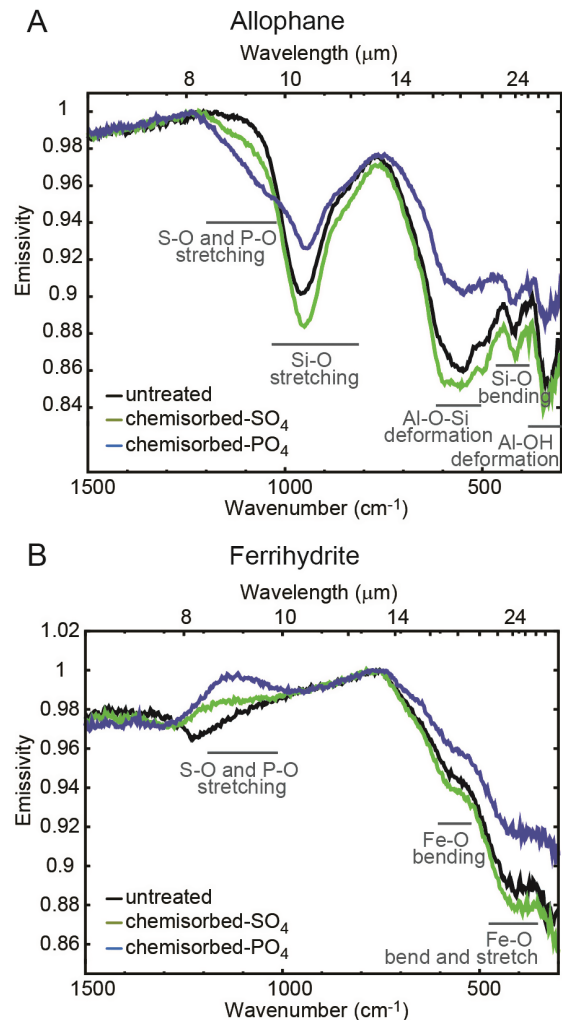


FIGURE 7. Thermal infrared emission spectra of (a) untreated, sulfate-chemisorbed, and phosphate-chemisorbed allophane, and (b) untreated, sulfate-chemisorbed, and phosphate-chemisorbed ferrihydrite.

TABLE 2. Band minima of allophane samples determined from corrected reflectance spectra

Sample	1.4 μm band minimum	1.9 μm band minimum
25 °C – Lab Air		
Untreated	1.413	1.939
Chemisorbed- SO_4	1.406	1.929
Chemisorbed- PO_4	1.406	1.918
25 °C – $\text{N}_{2(g)}$		
Untreated	1.413	1.939
Chemisorbed- SO_4	1.406	1.929
Chemisorbed- PO_4	1.406	1.918
110 °C – $\text{N}_{2(g)}$		
Untreated	1.400	1.936
Chemisorbed- SO_4	1.389	1.921
Chemisorbed- PO_4	1.381	1.916
220 °C – $\text{N}_{2(g)}$		
Untreated	1.378	1.929
Chemisorbed- SO_4	1.382	1.921
Chemisorbed- PO_4	1.380	1.921

vibrations and the shoulder at 600 cm^{-1} is from S-O and P-O bending vibrations (Farmer 1974; Cloutis et al. 2006). TIR emission spectra of compressed pellets of all ferrihydrite samples have broad bands at 550 and $300\text{--}450\text{ cm}^{-1}$ from Fe-O bending and Fe-O bending and stretching vibrations, respectively (Fig. 7b) (Vempati et al. 1990). The untreated ferrihydrite spectrum is similar to transmission TIR spectra of synthetic ferrihydrite samples (Bishop and Murad 2002), including an unassigned V-shaped weak band near 1300 cm^{-1} . The TIR emission spectra of sulfate- and phosphate-chemisorbed ferrihydrite samples are similar to the spectrum of the untreated ferrihydrite from $350\text{--}950\text{ cm}^{-1}$, but the chemisorbed ferrihydrite spectra have higher emissivity than the untreated ferrihydrite spectrum from $\sim 1000\text{--}1350\text{ cm}^{-1}$. This difference is a result of S-O and P-O stretching vibrations, which create Christiansen features [local maxima where the refractive index of the sample approaches that of the surrounding air (Conel 1969)] at $\sim 1150\text{ cm}^{-1}$. This feature is more apparent in the phosphate-chemisorbed ferrihydrite spectrum than the sulfate-chemisorbed ferrihydrite spectrum because more phosphate chemisorbed to the surface of ferrihydrite than sulfate ($1.6\text{ wt}\% \text{ SO}_4$ vs. $8.9\text{ wt}\% \text{ PO}_4$).

IMPLICATIONS FOR MARTIAN ORBITAL AND IN-SITU ANALYSES

Our analyses of sulfate and phosphate chemisorbed onto allophane and ferrihydrite with instruments that are laboratory counterparts to those on martian orbiter and landed missions show that these instruments have different detection limits for chemisorbed anionic species on the martian surface. EGA measurements, which were implemented as a part of the Phoenix lander thermal evolved gas analyzer (TEGA) and the MSL SAM instrument packages (Hoffman et al. 2008; Mahaffy et al. 2012), can distinguish allophane and ferrihydrite from their forms chemisorbed with sulfate because the method directly detects evolved S-bearing species at concentration levels expected in martian soils. Manifestations of chemisorbed sulfate and phosphate anions are also observed in VNIR spectra of allophane and TIR spectra of both allophane and ferrihydrite. VNIR spectra of ferrihydrite and XRD powder patterns and Mössbauer spectra of both npWP show no apparent evidence for chemisorption at the concentration levels of our experiments. We discuss these results in detail next, beginning with EGA data.

Laboratory EGA of untreated allophane and ferrihydrite show that both phases have similar, broad low-temperature H_2O releases with maxima near $120\text{ }^\circ\text{C}$, and allophane has a second maximum at $\sim 275\text{ }^\circ\text{C}$ not seen in data from ferrihydrite. This additional peak provides constraints for allophane vs. ferrihydrite identification in martian samples using $m/z\ 18$ data from SAM. Sulfate- or phosphate-chemisorbed ferrihydrite may be differentiated from anion-free ferrihydrite in $m/z\ 18$ data with the observation of a release near $440\text{ }^\circ\text{C}$ from the rapid transition from ferrihydrite to hematite.

With respect to SAM detection of chemisorbed sulfate or phosphate from S- or P-bearing mass fragments, only sulfate detection is viable because phosphate does not undergo thermal decomposition over SAM operating temperatures (ambient up to $1100\text{ }^\circ\text{C}$; Mahaffy et al. 2012). The $m/z\ 64$ EGA curves of sulfate-chemisorbed allophane and ferrihydrite show SO_2

releases from >900 and $\sim 400\text{--}800\text{ }^\circ\text{C}$, respectively, indicating that sulfate is indeed chemisorbed to the surfaces of the npWP. Thus, samples must be heated to temperatures in excess of $900\text{ }^\circ\text{C}$ to detect chemisorbed sulfate on allophane with SAM. To date, SAM thermal analyses have been limited to a maximum of $\sim 835\text{ }^\circ\text{C}$ (McAdam et al. 2014), permitting detection of chemisorbed sulfate on ferrihydrite but not allophane. In addition, SO_2 evolution from some Mg- or Ca-sulfate minerals may overwhelm the EGA signature of sulfate-adsorbed allophane if present in higher abundances. For example, epsomite undergoes sulfate decomposition at $970\text{ }^\circ\text{C}$ under SAM-like experimental conditions (Archer et al. 2013; Stern et al. 2013).

The $m/z\ 64$ EGA curve of sulfate-adsorbed ferrihydrite shows a series of SO_2 releases with maxima at ~ 400 , 490 , and $700\text{ }^\circ\text{C}$ (Fig. 4b), and all three temperatures are within the current operational range for SAM as discussed above. We attribute the higher ion current for the m/z release for sulfate-chemisorbed allophane compared to ferrihydrite to the higher concentration of chemisorbed sulfate to the former (4.5 and $1.6\text{ wt}\%$, respectively, from IC analyses). The presence of multiple $m/z\ 64$ releases might suggest the presence of multiple sulfate phases. However, our TEM results show that the chemisorbed ferrihydrite samples are homogenous and do not contain detectable separate sulfate phases.

To explain the $m/z\ 64$ releases at ~ 490 and $700\text{ }^\circ\text{C}$ in our experimental EGA data, we hypothesize that the S-bearing gas species released at $400\text{ }^\circ\text{C}$ from the decomposition of sulfate complexes chemisorbed to ferrihydrite surfaces reacted with the evolved H_2O vapor to form secondary ferric sulfates during the experiment. Alternatively, the S-bearing gas species may have reacted with the neo-formed hematite and chemisorbed to its surface. The subsequent decomposition of these secondary products caused the SO_2 releases at ~ 490 and $700\text{ }^\circ\text{C}$. Furthermore, crystalline and amorphous ferric sulfates show SO_2 releases from $\sim 500\text{--}800\text{ }^\circ\text{C}$ (McAdam et al. 2014; Ming et al. 2014), consistent with the two higher-temperature $m/z\ 64$ releases in sulfate-chemisorbed ferrihydrite, and other common sulfate minerals (e.g., Ca-, Mg-, and Al-sulfates) decompose at temperatures $>500\text{ }^\circ\text{C}$ (e.g., Lombardi 1984; Archer et al. 2013; Stern et al. 2013; McAdam et al. 2014; Ming et al. 2014). Thus, a $m/z\ 64$ release at $400\text{ }^\circ\text{C}$ in SAM data would distinguish sulfate chemisorbed onto ferrihydrite from discrete crystalline and amorphous ferric sulfates; however, this release has not been detected in SAM to date (McAdam et al. 2014, 2015; Ming et al. 2014). We hypothesize that similar reactions occur during the heating of phosphate-chemisorbed ferrihydrite (i.e., formation of secondary ferric phosphates or chemisorption of phosphate onto hematite); however, secondary ferric phosphates would not be detected with SAM-EGA because their thermal decomposition temperatures exceed the range of the experiments. In this case, the presence of a $m/z\ 18$ release at $\sim 440\text{ }^\circ\text{C}$, but the absence of a $m/z\ 64$ release at $400\text{ }^\circ\text{C}$ in SAM data may be evidence for chemisorbed phosphate on ferrihydrite.

Rocks and soils in Gale crater measured to date are comprised of as little as $10\text{--}15\text{ wt}\%$ X-ray amorphous material, based on 2σ errors from XRD analyses (Bish et al. 2013; Blake et al. 2013; Vaniman et al. 2014), to as much as $50\text{ wt}\%$, based on chemical calculations (Morris et al. 2015a). Calculations of sulfate

abundances in the amorphous component suggest it contains up to ~10 wt% SO_3 (Morris et al. 2015a), which implies that up to ~5 wt% SO_3 in each bulk sample can be attributed to the amorphous component (based on the assumption that 50 wt% of the sample is X-ray amorphous). Based on our laboratory EGA data, we expect to detect chemisorbed sulfate with SAM if that speciation is present in abundances of at least 1.3 wt% SO_3 in association with a ferrihydrite-like material.

XRD patterns of chemisorbed allophane and ferrihydrite are very similar to the untreated patterns, suggesting that chemisorption of sulfate and phosphate anions onto their surfaces does not affect their internal structures within detection limits. The only observable difference was for allophane where, at very low angles, the peak near 24 Å is more intense for the chemisorbed allophane than for the untreated allophane. Although there is a difference in the intensity of this low-angle peak between the untreated and chemisorbed allophane patterns, its location is outside the angular range of the CheMin instrument (Blake et al. 2012). CheMin can distinguish between untreated allophane and ferrihydrite on the basis of the positions of their broad diffraction peaks, which are within its angular range (Fig. 3), but the instrument cannot distinguish between their untreated and chemisorbed forms.

An important feature of the XRD patterns of allophane and ferrihydrite is the prominent rise in intensity at low angles because CheMin patterns of all martian samples measured to date display this feature. This increase in low-angle scattering intensity has been attributed to the regular packing of nanophase particles (van der Gaast et al. 1985; Bishop et al. 2013). However, the low-angle rise is not present in patterns of all amorphous materials (e.g., igneous glasses do not display this feature; Morris et al. 2015b). The increase in low-angle scattering intensity can be used to determine the presence (but not the identity) of npWP from CheMin data.

Mössbauer spectra of chemisorbed ferrihydrite measured at room temperature show the same doublet as the spectrum of untreated ferrihydrite. Mössbauer measurements of nanophase iron oxides at low temperatures can reduce the effects of small particle size and isomorphous substitution on the spectra so that they display a sextet instead of a doublet and nanophase iron oxides can be distinguished from one another (e.g., Pollard et al. 1992). Two-line ferrihydrite, as was studied here, displays a sextet in Mössbauer data when measured at extremely low temperatures (i.e., 4.2 K; Pollard et al. 1992); however, ferrihydrite displays a doublet at 77 K (Pollard et al. 1992). As such, we would not expect a sextet in Mössbauer data of ferrihydrite on Mars, so the Mössbauer spectra collected here are similar to those that would be collected on the martian surface. Furthermore, XRD patterns and TEM images indicate that crystalline structure is not affected by chemisorption, so we suggest that Mössbauer measurements at very low temperatures and modeling Mössbauer parameters from the subsequent sextets would not provide further information about the effects of chemisorption on crystal structure.

The chemisorption of sulfate or phosphate onto allophane or ferrihydrite does not introduce prominent spectral features that would readily permit VNIR spectral discrimination from their counterparts without chemisorbed anions. This suggests that unequivocal detection of chemisorbed sulfate and phosphate

is unlikely from orbital VNIR instruments like OMEGA and CRISM. However, the minima of the bands near 1.4 and 1.9 μm are at slightly shorter wavelengths for the chemisorbed allophane samples than those for the untreated allophane (Table 2). We suggest that this variation is the result of different relative H_2O abundances in the samples. The band near 1.4 μm has a contribution from H_2O , and the band near 1.9 μm is from H_2O . Chemisorption causes the removal of adsorbed H_2O , and as H_2O is removed from allophane, the bands at 1.4 and 1.9 μm shift to shorter wavelengths (Bishop et al. 2013). More phosphate is chemisorbed to allophane than sulfate in our samples, causing the 1.4 and 1.9 μm band minima in the phosphate-chemisorbed allophane to be at shorter wavelengths than the bands of sulfate-chemisorbed allophane. We speculate that this behavior is not seen in the NIR spectra of the ferrihydrite samples because ferrihydrite has less H_2O than allophane (~14 vs. ~21 wt%, respectively, for untreated samples as measured by thermal gravimetry) so that H_2O has a markedly lower contribution to NIR spectra of ferrihydrite than allophane.

VNIR spectra of the untreated and chemisorbed ferrihydrite show the band near 520 nm shifts to longer wavelengths and the relative reflectance near 800 nm diminishes with heating (Fig. 8), consistent with incipient bands for hematite at 630 and 860 nm (Morris et al. 1989). XRD patterns of the ferrihydrite samples heated to 220 °C show minor sharpening of the broad peaks, but do not display discrete hematite peaks (data not shown). These data, together with the absence of the H_2O spectral feature at 1.90 μm , suggest that the ferrihydrite partially dehydrated and/or dehydroxylated toward nanophase hematite with heating under dry $\text{N}_{2(g)}$.

Thermal-IR emission spectra of untreated allophane and ferrihydrite have broad spectral bands resulting from poor crystallinity. The chemisorption of both sulfate and phosphate onto allophane results in the presence of shoulder features on the high-frequency side of the Si-O stretching band from S-O and P-O bond vibrations, whereas sulfate and phosphate chemisorp-

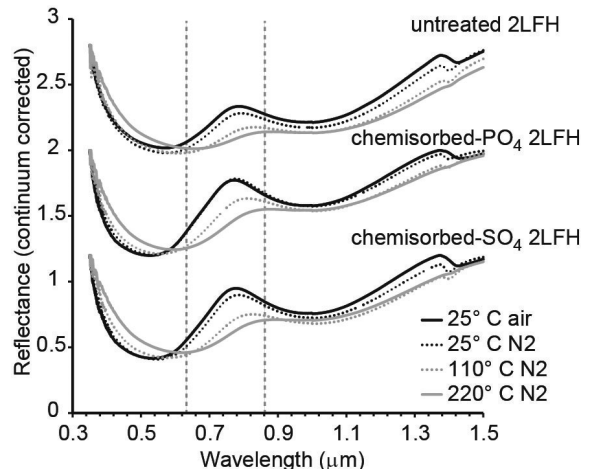


FIGURE 8. Laboratory visible/near-infrared spectra of untreated and chemisorbed ferrihydrite measured at room temperature and lab air and under $\text{N}_{2(g)}$ at room temperature, 110 °C, and 220 °C. Dashed vertical lines are at 630 and 860 nm. Spectra are offset for clarity.

tion on ferrihydrite causes an increase in the emissivity from $\sim 1000\text{--}1250\text{ cm}^{-1}$ because of Christiansen features associated with S-O and P-O stretching vibrations (e.g., Christensen et al. 2000; Cloutis et al. 2006; Lane et al. 2008, 2015). Mineral abundances in rocks and soils can be estimated from TIR spectra with linear mixing algorithms using a library of mineral spectra collected in the laboratory (Ramsey and Christensen 1998). Small differences between library member spectra can affect which member is selected by the algorithm (e.g., Rampe et al. 2012). Inclusion of spectra for allophane and ferrihydrite with and without chemisorbed sulfate and phosphate anions in TES and mini-TES spectral libraries provides a way to model for the presence or absence of these materials on the martian surface. We suggest that these features would be more easily recognized in IR data from landers and rovers (e.g., mini-TES on MER) rather than orbiters because of the large footprint of orbital spectrometers and the ability of landed missions to target individual samples. However, we hypothesize that chemisorbed sulfate and phosphate would be more difficult to recognize on high-silica allophane, as the Si-O stretching band may interfere with the S-O and P-O stretching vibrations. The laboratory TIR spectra of pressed pellets are relevant to npWP on the martian surface that are present as cohesive coatings on larger grains. If the npWP on the martian surface are fine grained, then their vibrational bands may be severely weakened by particle scattering (e.g., Salisbury and Wald 1992).

The presence of npWP on the martian surface has been previously inferred from orbital TES data (Rampe et al. 2012) and CRISM data (Weitz et al. 2014), in-situ Mössbauer spectroscopy (Morris et al. 2006a, 2006b, 2008), a combination of in-situ APXS chemical data and Mössbauer spectroscopy (Clark et al. 2005; Ming et al. 2006), and in-situ TIR spectroscopy by mini-TES (Ruff et al. 2011). MSL-CheMin XRD analyses confirm the presence of X-ray amorphous phases in all martian rocks and soil samples measured to date and indicate that amorphous phases are present in significant abundances (Bish et al. 2013; Vaniman et al. 2014; Morris et al. 2015a). The amorphous backgrounds in XRD patterns of the Rocknest soil and the Sheepbed mudstone appear to have one broad hump, rather than two as seen in allophane over the CheMin angular range, which suggests that allophane is not a major phase in the amorphous component. Additionally, the broad hump in CheMin data has a maximum near $30^\circ 2\theta$, which is inconsistent with the hump from ferrihydrite within the CheMin angular range ($\sim 40^\circ 2\theta$). MSL-SAM data from Rocknest and Sheepbed show broad low- T H_2O releases, consistent with hydrated nanophase materials like allophane and ferrihydrite (Leshin et al. 2014; Ming et al. 2014; Fig. 9a). Furthermore, SAM m/z 18 data of the Sheepbed mudstone have a shoulder near 275°C , consistent with allophane (Ming et al. 2014). However, calculations of the composition of the crystalline and amorphous components using mineralogy from CheMin and bulk chemistry from APXS show that the amorphous materials in Rocknest and Sheepbed are relatively poor in Al_2O_3 , so allophane would only be a minor phase if present at all (Dehouck et al. 2014; Morris et al. 2015a). SAM data from Rocknest and Sheepbed show SO_2 evolutions from $\sim 450\text{--}800^\circ\text{C}$, where Rocknest data have two peak temperatures at $\sim 500\text{--}550$ and $\sim 700\text{--}750^\circ\text{C}$ (McAdam et al. 2014) and Sheepbed data have peak temperatures at $600\text{--}625^\circ\text{C}$

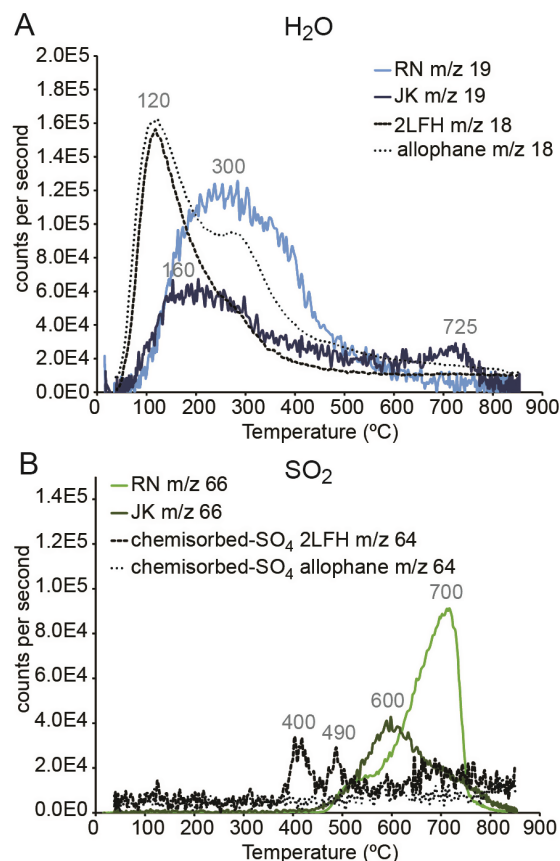


FIGURE 9. Evolved gas analysis data of (a) m/z 19 ($\text{H}_2\text{O}_{(g)}$) measured from Rocknest (RN) and John Klein (JK) samples by SAM and m/z 18 ($\text{H}_2\text{O}_{(g)}$) measured from npWP in the laboratory, and (b) m/z 66 ($\text{SO}_{2(g)}$) measured from Rocknest (RN) and John Klein (JK) samples by SAM and m/z 64 ($\text{SO}_{2(g)}$) measured from npWP in the laboratory. Traces from m/z 19 and 66 are displayed for Sample Analysis at Mars data because the detector was saturated for m/z 18 and 64. Runs 2 and 4 are displayed for RN and JK, respectively.

with a shoulder at $\sim 675^\circ\text{C}$ (Ming et al. 2014). Evolution of SO_2 from these samples is not consistent with sulfate chemisorbed onto ferrihydrite or allophane (Fig. 9b); however, SO_2 evolution from other npWP may occur in this temperature range, and these investigations are ongoing.

Amorphous phases are ubiquitous on Mars, so it is important to take the chemisorption properties of npWP into consideration when determining the speciation of S and P in rocks and soils on the martian surface. We suggest using high-temperature EGA with the SAM instrument to search for chemisorbed sulfate species in future samples measured at Gale crater, and the magnitude of the m/z 64 releases can help quantify the abundances of adsorbed sulfate. The shape of the amorphous background and the low-angle scattering intensity in CheMin patterns can be used to help constrain the identification of the nanophase weathering products present. The secondary mineralogy determined by CheMin may also be useful for estimating abundances of adsorbed sulfate and phosphate. Previous studies have characterized sulfate and phosphate adsorption isotherms with changing pH

for many npWP (e.g., Arai and Sparks 2001; Jara et al. 2006; Antelo et al. 2010). The identification by CheMin of minerals that are diagnostic of pH (e.g., jarosite, akaganeite) could help constrain pH and estimate the amount sulfate and phosphate chemisorbed onto npWP and further improve our understanding of the physico-chemical properties of amorphous material on Mars.

ACKNOWLEDGMENTS

We gratefully acknowledge the Mars Space Flight Facility at Arizona State University for the use of their Thermal-IR spectroscopy laboratory; Alicia Rutledge for her help measuring TIR spectra; Charlie Galindo, Dean Muir, and Chris Carrier for measuring IC data; Roy Christofferson for TEM analyses; DC Golden for his expert advice on nanophasic mineral syntheses and ion adsorption procedures; and Janice Bishop, Enver Murad, and an anonymous reviewer for their constructive comments on the manuscript. This work was funded by the NASA Mars Fundamental Research Program in an award to E.B. Rampe and R.V. Morris.

REFERENCES CITED

- Agresti, D.G., and Gerakines, P.A. (2009) Simultaneous fitting of Mars Mössbauer data. *Hyperfine Interactions*, 188, 113–120.
- Agresti, D.G., Dyar, M.D., and Schaefer, M.W. (2006) Velocity scales for Mars Mössbauer data. *Hyperfine Interactions*, 170, 67–74.
- Antelo, J., Fiol, S., Pérez, C., Mariño, S., Arce, F., Gondar, D., and López, R. (2010) Analysis of phosphate adsorption onto ferrihydrite using the CD-MUSIC model. *Journal of Colloid and Interface Science*, 347, 112–119.
- Arai, Y., and Sparks, D.L. (2001) ATR-FTIR spectroscopic investigation on phosphate adsorption mechanisms at the ferrihydrite-water interface. *Journal of Colloid and Interface Science*, 241, 317–326.
- Archer, P.D. Jr., Ming, D.W., and Sutter, B. (2013) The effects of instrument parameters and sample properties on thermal decomposition: Interpreting thermal analysis data from Mars. *Planetary Science*, 2, 2.
- Bibring, J.-P., and 42 colleagues (2004) OMEGA: Observatoire pour la Minéralogie, l'eau, les Glaces et l'Activité. In A. Wilson, Ed., *Mars Express: The Scientific Payload*. ESA Publications Division, Noordwijk, Netherlands, 37–49.
- Bish, D.L., and 19 colleagues (2013) X-ray diffraction results from Mars Science Laboratory: Mineralogy of Rocknest at Gale crater. *Science*, 341, <http://dx.doi.org/10.1126/science.1238932>.
- Bishop, J.L., and Murad, E. (2002) Spectroscopic and geochemical analyses of ferrihydrite from springs in Iceland and applications to Mars. In J.L. Smellie, and M.G. Chapman, Eds., *Volcano-Ice Interactions on Earth and Mars*. Geological Society, London, Special Publications, 202, 357–370.
- Bishop, J.L., Rampe, E.B., Bish, D.L., Abidin, Z., Baker, L.L., Matsue, N. and Henmi, T. (2013) Spectral and hydration properties of allophane and imogolite. *Clays and Clay Minerals*, 61, 57–74.
- Blake, D.F., and 21 colleagues. (2012) Characterization and calibration of the CheMin mineralogical instrument on Mars Science Laboratory. *Space Science Reviews*, 170, 341–399.
- Blake, D.F., and 45 colleagues (2013) Curiosity at Gale Crater, Mars: Characterization and analysis of the Rocknest sand shadow. *Science*, 341, <http://dx.doi.org/10.1126/science.1239505>.
- Borchardt, G. (1989) Smectites. In J.B. Dixon and S.B. Weed, Eds., *Minerals in Soil Environments*, p. 675–727. SSSA Book Series, Soil Science Society of America, Madison, Wisconsin.
- Catling, D.C., and Moore, J.M. (2003) The nature of coarse-grained crystalline hematite and its implication for the early environment of Mars. *Icarus*, 165, 277–300.
- Chevrier, V., Rochette, P., Mathé, P.-E., and Grauby, O. (2004) Weathering of iron-rich phases in simulated Martian atmospheres. *Geology*, 32, 1033–1036.
- Christensen, P.R., and Harrison, S.T. (1993) Thermal infrared emission spectroscopy of natural surfaces: Application to desert varnish coatings on rocks. *Journal of Geophysical Research*, 98, 19819–19834.
- Christensen, P.R., Bandfield, J.L., Hamilton, V.E., Howard, D.A., Lane, M.D., Piatek, J.L., Ruff, S.W., and Stefanov, W.L. (2000) A thermal emission spectral library of rock-forming minerals. *Journal of Geophysical Research*, 105, 9735–9739.
- Cichota, R., Vogeler, I., Bolan, N.S., and Clothier, B.E. (2007) Simultaneous adsorption of calcium and sulfate and its effect on their movement. *Soil Science Society of America Journal*, 71, 703–710.
- Clark, B., and 23 colleagues. (2005) Chemistry and mineralogy of outcrops at Meridiani Planum. *Earth and Planetary Science Letters*, 240, 73–94.
- Cloutis, E.A., and 11 colleagues. (2006) Detection and discrimination of sulfate minerals using reflectance spectroscopy. *Icarus*, 184, 121–157.
- Conel, J. (1969) Infrared emissivities of silicates: Experimental results and a cloudy atmosphere model of spectral emission from condensed particulate mediums. *Journal of Geophysical Research*, 74, 1614–1634.
- Dehouck, E., McLennan, S.M., Meslin, P.-Y., and Cousin, A. (2014) Constraints on abundance, composition, and nature of X-ray amorphous components of soils and rocks at Gale crater, Mars. *Journal of Geophysical Research*, 119, <http://dx.doi.org/10.1002/2014JE004716>.
- Elsheikh, M.A., Matsue, N., and Henmi, T. (2009) Effect of Si/Al ratio of allophane on competitive adsorption of phosphate and oxalate. *International Journal of Soil Science*, 4, 1–13.
- Farmer, V.C. (1974) *The infrared spectra of minerals*. Mineralogical Society, London, 539 p.
- Frost, R.L., Mills, S.J., and Erickson, K.L. (2004) Thermal decomposition of peisleyite: A thermogravimetry and hot stage Raman spectroscopic study. *Thermochimica Acta*, 419, 109–114.
- Gallini, S., Jurado, J.R., and Colomer, M.T. (2005) Synthesis and characterization of monazite-type Sr:LaPO₄ prepared through coprecipitation. *Journal of the European Ceramic Society*, 25, 2003–2007.
- Gálvez, N., Barrón, V., and Torrent, J. (1999) Effect of phosphate on the crystallization of hematite, goethite, and lepidocrocite from ferrihydrite. *Clays and Clay Minerals*, 47, 304–311.
- Hoffman, J.H., Chaney, R.C., and Hammack, H. (2008) Phoenix Mars Mission—The Thermal evolved gas analyzer. *Journal of the American Society for Mass Spectrometry*, 19, 1377–1383.
- Hunt, G.R., Salisbury, J.W., and Lenhoff, C.J. (1971) Visible and near-infrared spectra of minerals and rocks: IV. Sulphides and sulphates. *Modern Geology*, 3, 1–14.
- Ishiguro, M., Makino, T., and Hattori, Y. (2006) Sulfate adsorption and surface precipitation on a volcanic ash soil (allophanic andisol). *Journal of Colloid and Interface Science*, 300, 504–510.
- Janney, D.E., Cowley, J.M., and Busek, P.R. (2000) Transmission electron microscopy of synthetic 2- and 6-line ferrihydrite. *Clays and Clay Minerals*, 48, 111–119.
- Jara, A.A., Violante, A., Pigna, M., and de la Luz Mora, M. (2006) Mutual interactions of sulfate, oxalate, citrate, and phosphate on synthetic and natural allophanes. *Soil Science Society of America Journal*, 70, 337–346.
- Khare, N., Martin, J.D., and Hesterberg, D. (2007) Phosphate bonding configuration on ferrihydrite based on molecular orbital calculations and XANES fingerprinting. *Geochimica et Cosmochimica Acta*, 71, 4405–4415.
- Klingelhöfer, G., and 14 colleagues (2003) Athena MIMOS II Moessbauer spectrometer investigation. *Journal of Geophysical Research*, 108, 8067, <http://dx.doi.org/10.1029/2003JE002138>.
- Kwon, K.D., and Kubicki, J.D. (2004) Molecular orbital theory study on surface complex structures of phosphates to iron hydroxides: Calculation of vibrational frequencies and adsorption energies. *Langmuir*, 20, 9249–9254.
- Lane, M.D., Bishop, J.L., Dyar, M.D., King, P.L., Parente, M., and Hyde, B.C. (2008) Mineralogy of the Paso Robles soils on Mars. *American Mineralogist*, 93, 728–739.
- Lane, M.D., Bishop, J.L., Dyar, M.D., Hiroi, T., Mertzman, S.A., Bish, D.L., King, P.L., and Rogers, A.D. (2015) Mid-infrared emission spectroscopy and visible/near-infrared reflectance spectroscopy of Fe-sulfate minerals. *American Mineralogist*, 100, 66–82.
- Leshin, L.A., and 34 colleagues (2014) Volatile, isotope, and organic analysis of martian fines with the Mars Curiosity rover. *Science*, 341, <http://dx.doi.org/10.1126/science.1238937>.
- Lombardi, G. (1984) Thermal analysis in the investigation of zeolitized and altered volcanics of Latium, Italy. *Clay Minerals*, 19, 789–801.
- Mahaffy, P.R., and 84 colleagues. (2012) The Sample Analysis at Mars investigation and instrument suite. *Space Science Reviews*, 170, 401–478.
- Martin-Torres, F.J., and 24 colleagues. (2015) Transient liquid water and water activity at Gale crater on Mars. *Nature Geoscience*, 8, 357–361.
- McAdam, A.C., and 24 colleagues. (2014) Sulfur-bearing phases detected by evolved gas analysis of the Rocknest aeolian deposit, Gale Crater, Mars. *Journal of Geophysical Research*, 119, 373–393.
- McAdam, A.C., and 17 colleagues. (2015) Major volatiles from MSL SAM evolved gas analyses: Yellowknife Bay through lower Mount Sharp. 46th Lunar and Planetary Science Conference, Abstract 2323.
- Michalski, J.R., Kraft, M.D., Sharp, T.G., Williams, L.B., and Christensen, P.R. (2005) Mineralogical constraints on the high-silica martian surface component observed by TES. *Icarus*, 174, 161–177.
- Ming, D.W., and 16 colleagues. (2006) Geochemical and mineralogical indicators for aqueous processes in the Columbia Hills of Gusev crater, Mars. *Journal of Geophysical Research*, 111, <http://dx.doi.org/10.1029/2005JE002560>.
- Ming, D.W., and 57 colleagues. (2014) Volatile and organic compositions of sedimentary rocks in Yellowknife Bay, Gale Crater, Mars. *Science*, 343, <http://dx.doi.org/10.1126/science.1245267>.
- Morris, R.V., Agresti, D.G., Lauer, H.V. Jr., Newcomb, J.A., Shelfer, T.D., and Murali, A.V. (1989) Evidence for pigmentary hematite on Mars based on optical, magnetic, and Mössbauer studies of superparamagnetic (nanocrystalline) hematite. *Journal of Geophysical Research*, 94, 2760–2778.
- Morris, R.V., Golden, D.C., Bell, J.F. III, Lauer, H.V. Jr., and Adams, J.B. (1993) Pigmenting agents in Martian soils: Inferences from spectral, Mössbauer, and

- magnetic properties of nanophase and other iron oxides in Hawaiian palagonitic soil PN-9. *Geochimica et Cosmochimica Acta*, 57, 4597–4609.
- Morris, R.V., and 11 colleagues. (2000) Mineralogy, composition, and alteration of Mars Pathfinder rocks and soils: Evidence from multispectral, elemental, and magnetic data on terrestrial analog, SNC meteorite, and Pathfinder samples. *Journal of Geophysical Research*, 105, 1757–1817, <http://dx.doi.org/10.1029/1999JE001059>.
- Morris, R.V., Golden, D.C., Ming, D.W., Sheller, T.D., Jørgensen, L.C., Bell III, J.F., Graff, T.G., and Mertzman, S.A. (2001) Phyllosilicate-poor palagonitic dust from Mauna Kea Volcano (Hawaii): A mineralogical analog for magnetic Martian dust? *Journal of Geophysical Research*, 106, 5057–5083.
- Morris, R.V., and 19 colleagues. (2006a) Mössbauer mineralogy of rock, soil and dust at Gusev crater, Mars: Spirit's journey through weakly altered olivine basalt on the plains and pervasively altered basalt in the Columbia Hills. *Journal of Geophysical Research*, 111, <http://dx.doi.org/10.1029/2005JE002584>.
- Morris, R.V., and 23 colleagues (2006b) Mössbauer mineralogy of rock, soil, and dust at Meridiani Planum, Mars: Opportunity's journey across sulfate-rich outcrop, basaltic sand and dust, and hematite lag deposits. *Journal of Geophysical Research*, 111, <http://dx.doi.org/10.1029.2006JE02791>.
- Morris, R.V., and 16 colleagues. (2008) Iron mineralogy and aqueous alteration from Husband Hill through Home Plate at Gusev Crater, Mars: Results from the Mössbauer instrument on the Spirit Mars Exploration Rover. *Journal of Geophysical Research*, 113, <http://dx.doi.org/10.1029/2008JE003201>.
- Morris, R.V., et al. (2015a) Update on the chemical composition of crystalline, smectite, and amorphous components for Rocknest soil and John Klein and Cumberland mudstone drill fines at Gale crater, Mars. *Lunar and Planetary Science Conference XLVI*, 2622.
- Morris, R.V., and 6 colleagues. (2015b) Transmission X-ray diffraction (XRD) patterns relevant to the MSL ChemMin amorphous component: Sulfates and silicates. *Lunar and Planetary Science Conference XLVI*, 2434.
- Murchie, S., and 49 colleagues. (2007) Compact Reconnaissance Imaging Spectrometer for Mars (CRISM) on Mars Reconnaissance Orbiter (MRO). *Journal of Geophysical Research*, 112, <http://dx.doi.org/10.1029/2006JE002682>.
- Nanzyo, M., Dahlgren, R., and Shoji, S. (1993) Chemical characteristics of volcanic ash soils. In S. Shoji, M. Nanzyo, and R. Dahlgren, Eds., *Volcanic Ash Soils: Genesis, Properties and Utilization*, p. 145–188. *Developments in Soil Science*, Elsevier, Amsterdam.
- Ohashi, F., Wada, S.-I., Suzuki, M., Maeda, M., and Tomura, S. (2002) Synthetic allophane from high-concentration solutions: Nanoengineering of the porous solid. *Clay Minerals*, 37, 451–456.
- Parfitt, R.L. (1990) Allophane in New Zealand—A review. *Australian Journal of Soil Research*, 28, 343–360.
- Parfitt, R.L., and Hemmi, T. (1980) Structure of some allophanes from New Zealand. *Clays and Clay Minerals*, 28, 285–294.
- Pollard, R.J., Cardile, C.M., Lewis, D.G., and Brown, L.J. (1992) Characterization of FeOOH polymorphs and ferrihydrite using low-temperature, applied-field, Mössbauer spectroscopy. *Clays and Clay Minerals*, 27, 57–71.
- Rajan, S.S.S. (1979) Adsorption and desorption of sulfate and charge relationships in allophanic clays. *Soil Science Society of America Journal*, 43, 65–69.
- Rampe, E.B., Kraft, M.D., Sharp, T.G., Golden, D.C., Ming, D.W., and Christensen, P.R. (2012) Allophane detection on Mars with Thermal Emission Spectrometer data and implications for regional-scale chemical weathering processes. *Geology*, 40, 995–998.
- Ramsey, M.S., and Christensen, P.R. (1998) Mineral abundance determination: Quantitative deconvolution of thermal emission spectra. *Journal of Geophysical Research*, 103, 577–596.
- Ruff, S.W., Christensen, P.R., Barbera, P.W., and Anderson, D.L. (1997) Quantitative thermal emission spectroscopy of minerals: A laboratory technique for measurement and calibration. *Journal of Geophysical Research*, 102, 14,899–14,913.
- Ruff, S.W., and 10 colleagues. (2011) Characteristics, distribution, origin, and significance of opaline silica observed by the Spirit rover in Gusev crater, Mars. *Journal of Geophysical Research*, 116, <http://dx.doi.org/10.1029/2010JE003767>.
- Salisbury, J.W., and Wald, A. (1992) The role of volume scattering in reducing spectral contrast of reststrahlen bands in spectra of powdered minerals. *Icarus*, 96, 121–128.
- Schwertmann, U., and Cornell, R.M. (2000) *Iron Oxides in the Laboratory: Preparation and characterization*, 188 p. Wiley-VCH, Weinheim, Germany.
- Schwertmann, U., and Taylor, R.M. (1989) Iron oxides. In J.B. Dixon and S.B. Weed, Eds., *Minerals in Soil Environments*, p. 379–438. *SSSA Book Series*, Soil Science Society of America, Madison, Wisconsin.
- Stern, J.C., and 11 colleagues. (2013) Isotopic and geochemical investigation of two distinct Mars analog environments using evolved gas techniques in Svalbard, Norway. *Icarus*, 224, 297–308.
- Su, C., and Harsh, J.B. (1993) The electrophoretic mobility of imogolite and allophane in the presence of inorganic anions and citrate. *Clays and Clay Minerals*, 41, 461–471.
- Šubrt, J., Štengl, V., and Skokánek, M. (1992) Decomposition of ferrihydrite prepared from Fe(NO₃)₃ aqueous solutions under varying pH. *Thermochimica Acta*, 211, 107–119.
- van der Gaast, S.J., Wada, K., Wada, S.-I., and Kakuto, Y. (1985) Small-angle X-ray powder diffraction, morphology, and structure of allophane and imogolite. *Clays and Clay Minerals*, 33, 237–243.
- Vaniman, D.T., and 36 colleagues. (2014) Mineralogy of a mudstone at Yellowknife Bay, Gale Crater, Mars. *Science*, 343, <http://dx.doi.org/10.1126/science.1243480>.
- Vempati, R.K., Loeppert, R.H., Sittertz-Bhatkar, H., and Burghardt, R.C. (1990) Infrared vibrations of hematite formed from aqueous- and dry-thermal incubation of Si-containing ferrihydrite. *Clays and Clay Minerals*, 38, 294–298.
- Wada, K. (1987) Minerals formed and mineral formation from volcanic ash by weathering. *Chemical Geology*, 60, 17–28.
- (1989) Allophane and imogolite. In J.B. Dixon and S.B. Weed, Eds., *Minerals in Soil Environments*, p. 1051–1087. *SSSA Book Series*, Soil Science Society of America, Madison, Wisconsin.
- Wada, S.-I., Eto, A., and Wada, K. (1979) Synthetic allophane and imogolite. *The Journal of Soil Science*, 30, 347–355.
- Weitz, C.M., Bishop, J.L., Baker, L.L., and Berman, D.C. (2014) Fresh exposures of hydrous Fe-bearing amorphous silicates on Mars. *Geophysical Research Letters*, 41, 8744–8751.
- Willett, I.R., Chartress, C.J., and Nguyen, T.T. (1988) Migration of phosphate into aggregated particles of ferrihydrite. *Journal of Soil Science*, 39, 275–282.
- Zhu, M., Northrup, P., Chenyang, S., Billinge, S.J.L., Sparks, D.L., and Waychunas, G.A. (2014) Structure of sulfate adsorption complexes on ferrihydrite. *Environmental Science and Technology Letters*, 1, 97–101.

MANUSCRIPT RECEIVED MAY 6, 2015

MANUSCRIPT ACCEPTED SEPTEMBER 23, 2015

MANUSCRIPT HANDLED BY JANICE BISHOP